Technical University of Denmark

DTU

Controllable generation and manipulation of micro-bubbles in water with absorptive colloid particles by CW laser radiation

Angelsky, O. V.; Bekshaev, A. Ya.; Maksimyak, P. P.; Maksimyak, A. P.; Hanson, Steen Grüner; Kontush, S. M.

DTU Library
Technical Information Center of Denmark

Controllable generation and manipulation of micro-bubbles in water with absorptive colloid particles by CW laser radiation

O. V. ANGELSKY,[1,*] A. YA. BEKSHAEV,[2] P. P. MAKSIMYAK,[1] A. P. MAKSIMYAK,[1] S. G. HANSON,[3] AND S. M. KONTUSH[2]

[1]*Correlation Optics Department, Chernivtsi National University, 2, Kotsyubinsky Str., Chernivtsi 58012, Ukraine*
[2]*Research Institute of Physics, Odessa I.I. Mechnikov National University, Dvorianska 2, Odessa 65082, Ukraine*
[3]*DTU Fotonik, Department of Photonics Engineering, DK-4000 Roskilde, Denmark*
*angelsky@itf.cv.ua

Abstract: Micrometer-sized vapor-gas bubbles are formed due to local heating of a water suspension containing absorptive pigment particles of 100 nm diameter. The heating is performed by CW near-infrared (980 nm) laser radiation with controllable power, focused into a 100 μm spot within a 2 mm suspension layer. By changing the laser power, four regimes are realized: (1) bubble generation; (2) stable growth of the existing bubbles; (3) stationary existence of the bubbles and (4) the bubbles' shrinkage and collapse. This behavior is interpreted based on the temperature conditions. The generation and evolution of single bubbles and ensembles of bubbles with controllable sizes and numbers is demonstrated. The bubbles are grouped within the laser-illuminated region and form quasi-ordered structures. They can easily be moved and transported controlled by the focal spot. The results are useful for applications associated with the precise manipulation, sorting and specific delivery in nano- and micro-engineering problems.

References and links

1. G. Baffou, and H. Rigneault, "Femtosecond-Pulsed Optical Heating of Gold Nanoparticles," Phys. Rev. B **84**(3), 035415 (2011).
2. Z. Fang, Y. R. Zhen, O. Neumann, A. Polman, F. J. García de Abajo, P. Nordlander, and N. J. Halas, "Evolution of light-induced vapor generation at a liquid-immersed metallic nanoparticle," Nano Lett. **13**(4), 1736–1742 (2013).
3. D. A. Boyd, J. R. Adleman, D. G. Goodwin, and D. Psaltis, "Chemical separations by bubble-assisted interphase mass-transfer," Anal. Chem. **80**(7), 2452–2456 (2008).
4. D. A. Boyd, L. Greengard, M. Brongersma, M. Y. El-Naggar, and D. G. Goodwin, "Plasmon-assisted chemical vapor deposition," Nano Lett. **6**(11), 2592–2597 (2006).
5. C. Li, Z. Wang, P. I. Wang, Y. Peles, N. Koratkar, and G. P. Peterson, "Nanostructured copper interfaces for enhanced boiling," Small **4**(8), 1084–1088 (2008).
6. E. Lukianova-Hleb, Y. Hu, L. Latterini, L. Tarpani, S. Lee, R. A. Drezek, J. H. Hafner, and D. O. Lapotko, "Plasmonic nanobubbles as transient vapor nanobubbles generated around plasmonic nanoparticles," ACS Nano **4**(4), 2109–2123 (2010).
7. J. Kao, X. Wang, J. Warren, J. Xu, and D. Attinger, "A bubble-powered micro-rotor: conception, manufacturing, assembly and characterization," J. Micromech. Microeng. **17**(12), 2454–2460 (2007).
8. A. Hashmi, G. Yu, M. Reilly-Collette, G. Heiman, and J. Xu, "Oscillating bubbles: a versatile tool for lab on a chip applications," Lab Chip **12**(21), 4216–4227 (2012).
9. C. Zhao, Y. Liu, Y. Zhao, N. Fang, and T. J. Huang, "A reconfigurable plasmofluidic lens," Nat. Commun. **4**, 2305 (2013).
10. P. Marmottant, and S. Hilgenfeldt, "A bubble-driven microfluidic transport element for bioengineering," Proc. Natl. Acad. Sci. U.S.A. **101**(26), 9523–9527 (2004).
11. S. Lal, S. E. Clare, and N. J. Halas, "Nanoshell-Enabled Photothermal Cancer Therapy: Impending Clinical Impact," Acc. Chem. Res. **41**(12), 1842–1851 (2008).

12. M. Delcea, N. Sternberg, A. M. Yashchenok, R. Georgieva, H. Bäumler, H. Möhwald, and A. G. Skirtach, "Nanoplasmonics for Dual-Molecule Release through Nanopores in the Membrane of Red Blood Cells," ACS Nano **6**(5), 4169–4180 (2012).

13. P. Ghosh, G. Han, M. De, C. K. Kim, and V. M. Rotello, "Gold Nanoparticles in Delivery Applications," Adv. Drug Deliv. Rev. **60**(11), 1307–1315 (2008).

14. S. V. Oshemkov, L. P. Dvorkin, and V. Y. Dmitriev, "Trapping and manipulating gas bubbles in water with ultrashort laser pulses at a high repetition rate," Tech. Phys. Lett. **35**(3), 282–285 (2009).

15. V. Kotaidis, C. Dahmen, G. von Plessen, F. Springer, and A. Plech, "Excitation of nanoscale vapor bubbles at the surface of gold nanoparticles in water," J. Chem. Phys. **124**(18), 184702 (2006).

16. M. T. Carlson, A. J. Green, and H. H. Richardson, "Superheating water by CW excitation of gold nanodots," Nano Lett. **12**(3), 1534–1537 (2012).

17. I. Akhatov, N. Vakhitova, A. Topolnikov, K. Zakirov, B. Wolfrum, T. Kurz, O. Lindau, R. Mettin, and W. Lauterborn, "Dynamics of laser-induced cavitation bubbles," Exp. Therm. Fluid Sci. **26**(6-7), 731–737 (2002).

18. S. F. Rastopov, and A. T. Sukhodol'sky, "Cluster nucleation in the process of CW laser induced thermocavitation," Phys. Lett. A **149**(4), 229–232 (1990).

19. J. C. Ramirez-San-Juan, E. Rodriguez-Aboytes, A. E. Martinez-Canton, O. Baldovino-Pantaleon, A. Robledo-Martinez, N. Korneev, and R. Ramos-Garcia, "Time-resolved analysis of cavitation induced by CW lasers in absorbing liquids," Opt. Express **18**(9), 8735–8742 (2010).

20. J. P. Padilla-Martinez, C. Berrospe-Rodriguez, G. Aguilar, J. C. Ramirez-San-Juan, and R. Ramos-Garcial, "Optic cavitation with CW lasers: A review," Phys. Fluids **26**(12), 122007 (2014).

21. G. Baffou, J. Polleux, H. Rigneault, and S. Monneret, "Super-heating and micro-bubble generation around plasmonic nanoparticles under cw illumination," J. Phys. Chem. C **118**(9), 4890–4898 (2014).

22. O. V. Angelsky, A. Ya. Bekshaev, P. P. Maksimyak, A. P. Maksimyak, S. G. Hanson, and C. Yu. Zenkova, "Self-action of continuous laser radiation and Pearcey diffraction in a water suspension with light-absorbing particles," Opt. Express **22**(3), 2267–2277 (2014).

23 C. Mätzler, MATLAB Functions for Mie Scattering and Absorption, Version 2, IAP Research Report, No. 2002–11 (Institut für angewandte Physik, Universität Bern, 2002).

24. N. V. Tsederberg, *Thermal Conductivity of Gases and Liquids* (Massachusetts Institute of Technology, 1965).

25. M. Abramovitz, and I. Stegun, *Handbook of Mathematical Functions* (National Bureau of Standards, Applied Mathematics Series, 55 1964).

26. C. Yang, C. Yang, T. Dabros, D. Li, J. Czarnecki, and J. H. Masliyah, "Measurement of the Zeta Potential of Gas Bubbles in Aqueous Solutions by Microelectrophoresis Method," J. Colloid Interface Sci. **243**(1), 128–135 (2001).

27. W. Jia, S. Ren, and B. Hu, "Effect of Water Chemistry on Zeta Potential of Air Bubbles," Electrochem. Sci. **8**, 5828–5837 (2013).

28. M. Chaplin, "Theory vs Experiment: What is the Surface Charge of Water?" Water **1**, 1–28 (2009).

29. Y. Y. Geguzin, *Bubbles* (Moscow, Nauka, 1985) (In Russian).

30. N. B. Vargaftik, B. N. Volkov, and L. D. Voljak, "International tables of the surface tension of water," J. Phys. Chem. Ref. Data **12**(3), 817–820 (1983).

31. A. Y. Bekshaev, "Subwavelength particles in an inhomogeneous light field: optical forces associated with the spin and orbital energy flows," J. Opt. **15**(4), 044004 (2013).

32. G. K. Batchelor, *An Introduction to Fluid Dynamics* (Cambridge University, 1967).

33. Viscopedia: A free encyclopedia for viscosity, "Water," http://www.viscopedia.com/viscosity-tables/substances/water.

34. E. Flores-Flores, S. A. Torres-Hurtado, R. Páez, U. Ruiz, G. Beltrán-Pérez, S. L. Neale, J. C. Ramirez-San-Juan, and R. Ramos-García, "Trapping and manipulation of microparticles using laser-induced convection currents and photophoresis," Biomed. Opt. Express **6**(10), 4079–4087 (2015).

35 M.-R. Kalus, N. Bärsch, R. Streubel, E. Gökce, S. Barcikowski, and B. Gökce, "How persistent microbubbles shield nanoparticle productivity in laser synthesis of colloids – quantification of their volume, dwell dynamics, and gas composition," Phys. Chem. Chem. Phys. **19**, Accepted Manuscript (2017).

1. Introduction

Gas and vapor bubbles of nano- and micrometric sizes in aqueous solutions are interesting for many fundamental and applied research problems: thermodynamic studies of liquid superheating and phase transitions in nano-scale [1–6], microhydraulic and micromachinery manipulation [7,8], microoptics [9], diverse biomedical applications including cell investigations, sorting, precise drug delivery and therapy [11–13].

Therefore, the task of controllable bubble generation is very important, and the laser radiation provides suitable and efficient approaches for its fulfillment. For a long time, the bubble emergence under the pulsed laser illumination was the main object of interest [6,14–17]. Large amount of energy supplied by the short laser pulse results in very rapid water evaporation and bubble growth followed by the high-speed collapse with possible rebounds

and energy release in form of luminescence and/or shock waves (optical cavitation). However, the bubble generation by CW laser radiation is more suitable for various technological purposes. In this case, a rich and intricate dynamic behavior with fluid superheating and explosive bubble formation is possible [18–20], but more attractive is the availability of near-stationary regimes of bubble evolution permitting their detailed investigation and control [2,21]. It is the near-stationary long-living bubbles that provide exclusive possibilities for the precise mass transfer, highly selective chemical actions, targeted transport of biological cells and species, creation of adjustable microoptical systems, etc [3,4,6,8–13].

In this work, we demonstrate a simple scheme for generation of microbubbles and their ensembles in water suspension containing colloidal light-absorbing nanoparticles (diluted suspension of black ink for jet printers) based on the suspension heating by the moderately focused beam of the near-IR laser. The bubbles are formed around the ink particles due to the superheated water evaporation; however, in contrast to [2], the great number of closely situated heating centers (particles) provides macroscopic collective effects of the inhomogeneous temperature distribution, which can be suitably regulated by the incident laser power. As a result, we demonstrate the possibility of controllable growth of bubbles up to sub-millimeter size. Under special heating regimes, based on the special temporal variation of the incident laser power, generation of spatially-ordered systems of bubbles with controllable size distribution is shown. The bubbles obtained and their ensembles show high stability and can exist for a long time provided that the illumination conditions are maintained. Their spatial localization is fixed within the bright spot, and the bubbles can be transported across the liquid volume together with the focal region of the beam.

2. Experiment

2.1. Experimental equipment

The scheme of the experimental setup is presented in Fig. 1. The radiation of the semiconductor laser (Wavespectrum, WSLD-980-004-C, wavelength in vacuum $\lambda = 980$ nm, maximum power 4 W) was focused in the cuvette with the water suspension. The cuvette is formed by the bottom glass plate and the glass ring with height 2 mm and the inner diameter $D = 10$ mm. The laser radiation was focused within a cone angle 5°, and without spatial filtering the focal spot diameter

$$2b \approx 100\,\mu\mathrm{m} \tag{1}$$

was formed. In such conditions (wavenumber $k = 2\pi /\lambda = 6.41 \cdot 10^4$ cm^{-1}), the Rayleigh range of the focused beam can be estimated as

$$kb^2 \sim 16\,\mathrm{mm}, \tag{2}$$

so the focal depth is rather large and the beam diameter within the cuvette is practically constant.
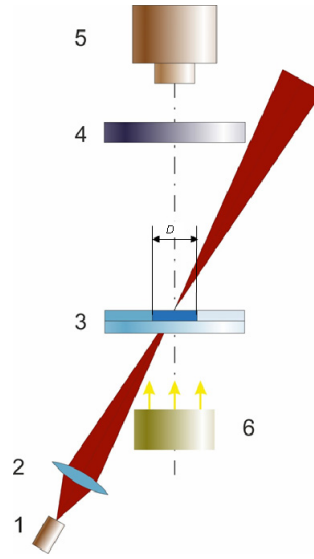
Fig. 1. The experimental setup: (1) IR laser, (2) objective, (3) cuvette with the water suspension of absorbing nanoparticles, (4) spectral filter to stop the IR radiation, (5) CCD camera, (6) white-light source for visible illumination.

The processes in the cuvette were visualized by white-light illumination and registered by the 1.3 megapixel CCD camera with removed IR-protective cover glass, which permitted us to observe the bubbles illuminated by the visible light as well as the IR laser beam trace inside the cuvette. In case of normal incidence of the IR laser beam, the IR power reaching the CCD camera was too high even in the presence of the IR filter, so the heating IR radiation was directed to the cuvette obliquely (see Fig. 1), approximately at an angle 15°, and the camera received only the scattered IR light. The receiving optical system was designed to image the near-surface layer of the cuvette suspension. The IR laser power was adjustable within the range 0.1 W to 3 W.

The cuvette contained the water suspension of the black pigment ink (InkTec Corporation [22]). Each pigment particle consists of a spherical polymer core (refraction index $n_c = 1.59$) covered with resin coating (shell), refraction index $n_s = 1.58 + 0.74i$. The mean core radius is $a_c = 80$ nm and the absorbing shell thickness is $a_s = 20$ nm, so the suspension contains spherical coated particles with mean radius $a_p = a_c + a_s = 100$ nm. In the water ambient medium with refraction index

$$n_w = 1.33,\tag{3}$$

and for the above-specified vacuum wavelength of the laser radiation, the Mie theory [23] predicts the following extinction σ_{ext} and absorption σ_{abs} cross sections:

$$\sigma_{ext} = 0.587\sigma, \quad \sigma_{abs} = 0.543\sigma,\tag{4}$$

where geometric cross section of the particle equals

$$\sigma = \pi a_p^2 = 3.14 \times 10^{-10}\,\text{cm}^2.\tag{5}$$

In our experiments, the diluted ink suspension was used with measured absorption coefficient via the light attenuation,

$$\alpha = 0.60\,\text{cm}^{-1}.\tag{6}$$

This value corresponds to the particles' concentration

$$N = \frac{\alpha}{\sigma_{abs}} \approx 0.35 \cdot 10^{10} \, \text{cm}^{-3}. \tag{7}$$

Hence, the volume per particle is $N^{-1} = 2.8 \cdot 10^{-10}$ cm^3 and the mean distance between the particles constitutes $N^{-1/3} \approx 6.6 \cdot 10^{-4}$ cm = 6.6 mm. Assuming the particle density ~1 g/cm^3, this corresponds to an ink pigment concentration $(4/3)\pi a_p^3 N \approx 1.5 \cdot 10^{-5}$ g/cm^3.

2.2. Model of the temperature conditions

Each particle efficiently absorbs the incident radiation and the absorbed energy is eventually transmitted to the ambient water causing a temperature increase. Due to the small inter-particle distance, an average temperature T is established in a small volume containing many particles, and the temperature distribution can be calculated via the Fourier law for the thermal conductivity [24]. In the stationary conditions this is described by the equation

$$\kappa \nabla^2 T + F = 0, \tag{8}$$

where κ is the thermal conductivity coefficient and F is the function of coordinates describing the heat source density. When the light beam propagates through the medium, the energy absorbed per unit volume is αI, where I is the beam intensity (energy flow density). Obviously, with the absorption coefficient (6), the beam energy decreases rather slightly upon the beam propagation within the cuvette; additionally, in the first approximation we may neglect the beam obliquity and assume that the cuvette is illuminated in its center and, allowing for the relatively high focal depth (2), consider $I = I(r)$ as a function of only one spatial coordinate: the radial distance from the cuvette axis r, which is supposed to be Gaussian (this, again, is a rather arbitrary approximation since the beam of the semiconductor laser experienced no spatial filtering). Then the source function can be expressed as

$$F(r) = \alpha I(r) = \frac{\alpha Q_0}{\pi b^2} \exp\left(-\frac{r^2}{b^2}\right), \tag{9}$$

where Q_0 is the incident beam power and b is the focal (1/e)-intensity spot radius (see Eq. (1)). Now we accept further approximations by treating the problem of Eq. (8) as circularly-symmetric with T depending only on r; this admission includes also the hypothesis that the heat transfer via the cuvette bottom and the air above the water surface is not important, and that the prevailing way of energy diffusion is through the water volume with thermal conductivity coefficient $\kappa \approx 0.6$ W/(m·K). With the additional requirement that at the cuvette side wall ($r = D/2$) the temperature is fixed, $T = T_D$ (usually this is the room temperature, $T_D = 300$ K), the solution to Eqs. (8), (9) follows in the form

$$\Delta T(r) \equiv T(r) - T_D = \frac{\alpha Q_0}{4\pi\kappa}\left[\text{Ei}\left(-\frac{r^2}{b^2}\right) - \text{Ei}\left(-\frac{D^2}{4b^2}\right) - 2\ln\left(\frac{2r}{D}\right)\right], \tag{10}$$

where $\text{Ei}(-z) = -\int_z^\infty \frac{\exp(-t)}{t}dt$ is the integral exponent function [25]. The temperature distribution (10) for different values of the laser power used in our experiment is illustrated by Fig. 2.
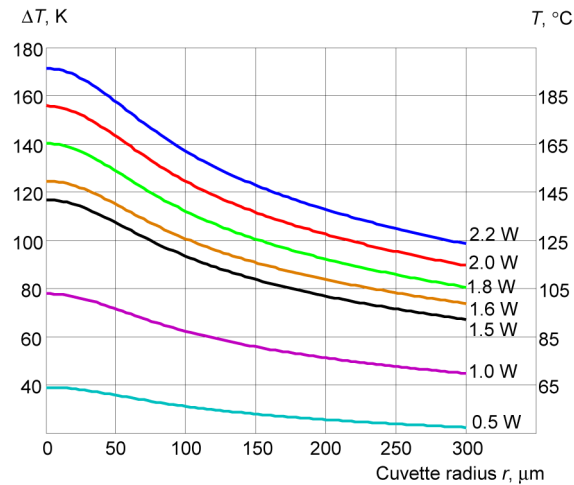
Fig. 2. Temperature distribution in the near-axial region of cuvette 3 of Fig. 1 calculated via Eq. (10) under conditions (1) and (6) for D = 10 mm, $\kappa \approx 0.6$ W/(m·K) and different values of the incident laser power Q_0 indicated near the curves. Left scale: local temperature excess with respect to its value at the cuvette wall ($r = D/2$); right scale: true local temperature.

3. Results and discussion

3.1. Principles of the bubble generation and growth

According to the known ideas [2,19–21], the bubble nucleation initially occurs near a single absorbing nanoparticle in conditions of water superheating when the local temperature exceeds the standard boiling temperature 100 °C. Therefore, the theoretical superheating limit – critical conditions for water T_C = 374 °C at pressure P_C = 22.09 MPa – normally is not realized, and the new phase (bubbles), due to the presence of liquid-solid interfaces, adsorbed gas molecules and other imperfections, appear at lower temperatures, about T_g = 200 °C [2,21]. In principle, each particle in the considered suspension is a separate heating source and serves as a center of bubble nucleation in which both the water vapor and the air gases dissolved in the water play important roles [2,21]. However, because of statistical fluctuations, the nucleation starts as a random event [19,20], and most probably occurs when the local conditions are especially favorable, e.g. when due to Brownian motion two or more particles appear anomalously close to each other and cause the local "excess" of released energy. Probability of such an event is higher in regions with higher ambient temperature, which, in turn, is a result of "collective" action of separate temperature fields of the individual particles that are distributed rather densely in the suspension. The resulting mean temperature distribution was discussed in Sec. 2.2.

Figure 2 shows that the ambient temperature close to T_g = 200 °C can occur in the cuvette center if the laser power $Q_0 \geq 2.2$ W. Indeed, in our experiments the value Q_0 = 2.2 W was the threshold below which new bubbles did not appear. If the power exceeds 2.2 W, the bubbles emerge, and normally in growing number. Once the power decreases again below the threshold, generation of new bubbles stops but the evolution of the existing ones can be traced. Observing the consecutive events of the bubble generation in real time, we could fix a desirable number of bubbles by decreasing the incident power to suppress generation of more bubbles.

3.2. Multiple bubble generation

Just after the birth, the bubbles "feel" the mean temperature field of Fig. 2 (curve marked 2.2 W), i.e. at the ambient temperature T_g = 200 °C, and continue to grow. When their sizes reach

several micrometers, the bubbles begin to interact. To study this interesting situation experimentally, we maintained the threshold power until several bubbles appear in the microscope view field, and then switched the laser power below 2.2 W. Further evolution depends on the bubbles' number and the incident laser power.

An example of the bubble ensemble observed 30 s after the generation started is presented in Fig. 3 (see also Visualization 1). It is seen that the bubbles possess different sizes, 10 to 30 mm, which reflects different times elapsed from their birth and different temperature conditions in which they are situated. All the bubbles are floating in the near-surface layer (some of them, initially generated in the liquid volume, rapidly move up due to the Archimedean force). However, they do not coalesce and do not cross nor adhere to the water–air boundary, which can be explained by the electric charges accumulated at the bubble's and water surfaces. As is known [26,27], due to the dipole nature of the water molecules, gas bubbles in aqueous media accumulate negative surface charges, and the electric double layer is formed with diffuse distribution of the oppositely charged (positive) ions in the near-bubble water volume. As a result, the appearing electrostatic force prevents the gas bubbles from close encounters. A similar double electric layer at the water–air interface [28] keeps the bubbles below the liquid surface.
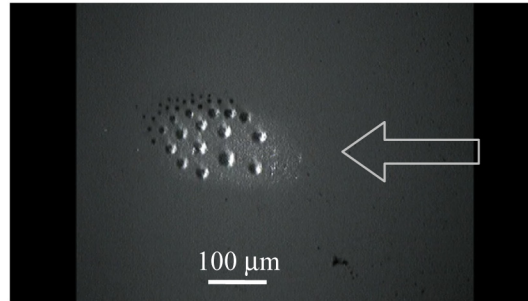

100 μm

Fig. 3. View of the ensemble of bubbles 30 seconds after the generation by the IR beam of power 2.2 W. Note the overall displacement of the bubbles with respect to the bright spot, which is caused by the convective water flow schematically indicated by the arrow (Visualization 1).

The bubbles always keep together within or very close to the IR-illuminated region. It is not surprising that the bubbles can be observed only in the high-temperature region outside which they simply cannot exist – but they remarkably never diffuse to the rest of the cuvette volume. Visualization 1 shows that even the liquid flow with velocity v = 150 mm/s (which was excited because of slight heating asymmetry) cannot capture the bubbles. This strong adherence of the bubbles to the laser spot can be ascribed to the temperature dependence of the surface tension of water due to which the bubbles experience the force [29]

$$\mathbf{F}_{\mathrm{ST}} = -\pi R^2 \frac{d\gamma}{dT} \nabla T, \tag{11}$$

where R is the bubble radius and γ is the surface tension. According to the Tables [30], for water at boiling temperature $d\gamma/dT = -0.19\cdot10^{-3}$ N/(m·K). This negative value in combination with Eq. (11) means that the bubbles tend to move towards the more heated region.

For quantitative estimates, note that in accordance with Fig. 2, the temperature gradient in the cuvette can reach $|\nabla T| = |dT/dr| \approx 2\cdot10^{5}\cdot[Q_0]$ K/m where $[Q_0]$ is the incident IR power in Watts. Then for a bubble with R = 5 mm the force (11) amounts to $3.0\cdot10^{-9}[Q_0]$ N. Of course, this is the maximum force exerted on a bubble that is situated at the position of the steepest slope of the temperature curve ($r \approx$ 150 mm, see Fig. 2) but it is clear that for any

position near of within the focal spot, the force (11) is sufficient to keep the bubbles within the most heated region.

To confirm this conclusion, we consider another force that acts under these conditions: the electromagnetic gradient force, which must "push" the bubbles away from the laser beam spot since the gas (vapor) refraction index 1 is less than the water refraction index. This force can be estimated in the dipole approximation as [31]

$$\mathbf{F}_{EG} = 2\pi R^3 \frac{1-\varepsilon}{1+2\varepsilon}\nabla W, \quad |\mathbf{F}_{EG}| = \frac{4n_w}{c}\frac{R^3}{b^3}\frac{1-\varepsilon}{1+2\varepsilon}Q_0\left[\frac{r}{b}\exp\left(-\frac{r^2}{b^2}\right)\right], \quad (12)$$

where $W(r) = (n_w/c)I(r)$ is the electromagnetic energy density, n_w is the water refraction index (see Eq. (3)), c is the light velocity in vacuum, $\varepsilon = n_w^2$ and Eq. (9) has been used. Under the conditions of the above paragraph and with $b = 50$ mm (see Eq. (1)), the second formula (12) gives that at its maximum ($r = b/\sqrt{2}$) the optical force reaches $1.3\cdot10^{-12}[Q_0]$, which is really negligible compared to the force (11). Actually, the ray-optics approximation is more relevant in this case but one can show that it will only introduce a numerical multiplier of the order of unity into Eq. (12), which does not affect the conclusion on the gradient force weakness. Additionally, the similar considerations show that another electromagnetic force, the light-pressure force which acts in the longitudinal direction (towards the liquid surface), is also very small in comparison with the vertical forces of thermal, electrostatic or mechanical origin that act in this system.

Visualization 1 supplies an additional manifestation of the temperature gradient force (11) that is connected with the peculiar distribution of bubbles with different sizes. One can see that large bubbles take positions in the central part of the illuminated area, where the temperature gradient is low, while small ones are concentrated at the spot periphery and mostly in its rear part with respect to the liquid flow. A possible reason for this is that the bubbles experience a dragging force from the flow described by the Stokes formula [32]

$$F_S = 6\pi R\eta v, \quad (13)$$

where $\eta = 0.35\times10^{-3}$ Pa·s is the water viscosity [33]. Obviously, for the same ambient conditions, small bubbles require higher temperature gradient, and, additionally, directed against the flow, to avoid its capturing influence, than the large ones do. At the same time, the small bubbles evidently "feel" the flow action and show certain flow-induced redistributions, provided that they do not invoke the opposing action of the temperature gradient.

Thus, it is the temperature inhomogeneity that keeps the bubbles together within the spot of the IR radiation, and the electrical double layers produce certain short-range repulsive forces between the bubbles. The situation looks similar to that of crystal or liquid structure where the competition of attractive and repulsive interactions leads to self-organization: densely packed bubbles form quasi-ordered structures that "fill" the IR-illuminated spot and are stable to mechanical perturbations. This fact is promising for diverse manipulation techniques as it permits easy and precise transportation of the bubble ensembles to any desirable position.

3.3. Single bubble regime

In case of multiple bubble generation considered in the previous section, bubble growth is limited by their sizes: once several bubbles appear in the IR-illuminated region and the power is switched slightly below the threshold $Q_0 = 2.2$ W, they still grow until the "packed" configuration of Fig. 3 and Visualization 1 is accomplished. In more detail, regularities of the bubble growth can be studied via the simpler situation that is realized when only one "survived" bubble is observed.

This is possible because in the regime of bubbles' generation, they appear at random but consecutive moments of time, and in many cases we were able to detect the emergence of the first bubble after which the laser power Q_0 was reduced below the threshold 2.2 W. Then the generation of new bubbles is suppressed but the existing bubble continues to grow with a rate depending on the actual Q_0 value until it expands practically over the whole IR-illuminated region (see Figs. 4 and 5). However, at $Q_0 = 1.5$ W the bubble growth stops and below 1.5 W reverses to shrinkage; this is the second threshold power at which the water heating becomes insufficient to support the stationary bubbles. For $Q_0 < 1.5$ W, the lower Q_0, the faster is the bubble collapse and at $Q_0 = 0.5$ W the bubbles vanish instantly (in view of the low-time-resolution technique of our experiment, it occurs in less than a second).
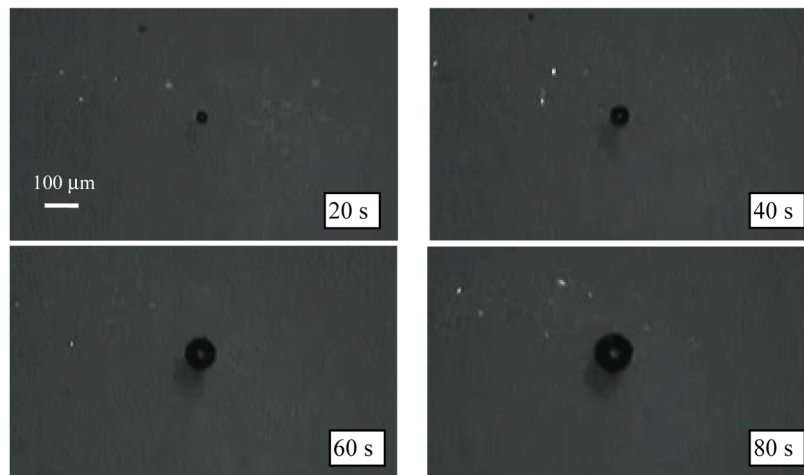

Fig. 4. Consecutive views of the growing bubble at the IR radiation power $Q_0 = 2.0$ W; the inserts indicate the time interval since the bubble birth.
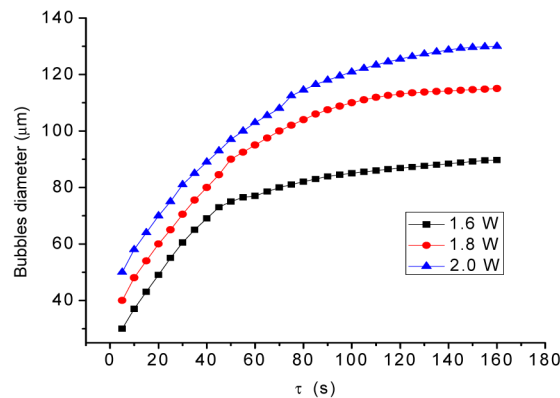

Fig. 5. Time dependencies of the bubble sizes for different IR laser powers indicated in the insert (cf. Fig. 2).

These regularities can be interpreted based on the data in Fig. 2. The position of the curve for $Q_0 = 1.5$ W suggests that the temperature $T_B = 145$ °C is necessary for the bubble maintenance. It is natural to suppose that the bubble grows until its boundary reaches the region where the local temperature $T(r) = T_B$. According to Fig. 2, this means that at $Q_0 = 1.6$ W the stationary (final) bubble diameter is about 80 mm, which agrees with Fig. 5. For $Q_0 = 1.8$ W and $Q_0 = 2.0$ W, the similar reasoning gives the final bubble size ~150 mm and ~220 mm, respectively. The discrepancy with the really observed values presented in Fig. 5 can be

explained by the idealizations made upon the calculation of the temperature distribution in Fig. 2. Moreover, the presence of a large bubble essentially modifies the conditions for the light absorption and the heat transfer; actually, the temperature analysis in Sec. 2.2 is adapted to the "initial" heating stage that regulates the bubble birth, and its application to the later stages of the bubble growth can hardly bring more than qualitative results.

The considered principles of the single-bubble evolution provide additional arguments for the discussion of the bubble ensembles. First, they are fully applicable to "rarified" bubble groups that are realized until separate simultaneously existing bubbles are small enough so that their electric double layers do not interact. Indeed, Fig. 6 represents the synchronous growth of four nearly identical bubbles that is rather similar to the single-bubble growth in Fig. 4. Note, however, that the current bubble sizes in the "group regime" are smaller than those observed in the single-bubble regime and presented in Fig. 5, black curve. Figure 6 also demonstrates that separate bubbles of the ensemble try to be situated at largest possible distances between each other, compatible with the necessary temperature level.

Second, in relation to the dense bubble ensembles described in Sec. 3.2, a rough but remarkable correspondence exist between the "final bubble sizes" 80 mm, 150 mm and 220 mm in Fig. 5 and the areas occupied by densely packed bubbles at the incident power 1.6 W, 1.8 W and 2.0 W. This is to be expected because the smaller bubbles forming the ensembles require for their stability the same temperature conditions that are necessary for the large bubbles discussed in Fig. 5. We saw that the single bubble size was limited by the region with temperature $T > T_B \approx 145°C$, and the small ones occupy approximately the same area.
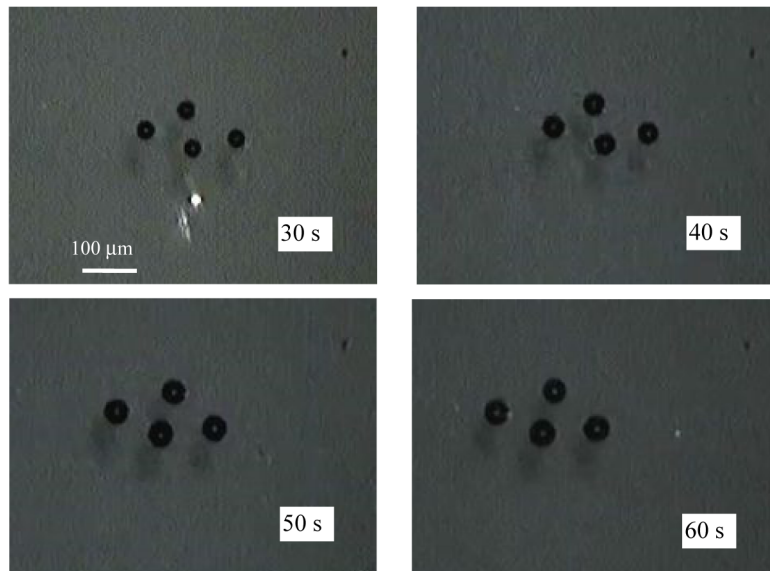

Fig. 6. Synchronous growth of four bubbles at the IR radiation power 1.6 W.

4. Controlled generation of the bubble ensemble

The method of the bubble generation described in this work provides efficient means for additional control of the number, sizes and other parameters of the created bubbles. To illustrate the general approach for deliberate control of the bubble generation process, we present an example of the bubble ensemble consisting of two distinct size fractions (Fig. 7, Visualization 2).
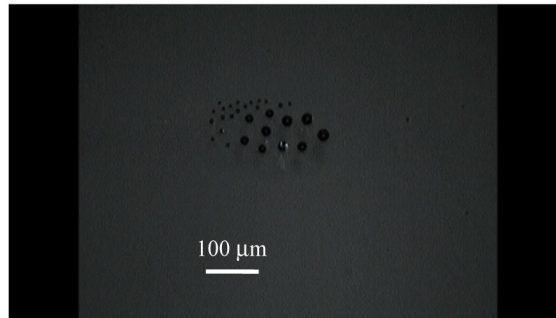
Fig. 7. The ensemble of bubbles with two scales, 15 mm and 40 mm (Visualization 2).

The two fractions were obtained on the base of regularities described by the curves in Fig. 5. Initially, a certain number of bubbles is generated at the threshold laser power $Q_0 = 2.2$ W. Afterwards, the power is decreased to 1.8 W, and in this regime the bubbles are "grown" but to the size that is smaller than the necessary final size. At that moment, the power is again switched above the threshold 2.2 W for a short time during which the second fraction of bubbles is generated, and after turning back to 1.8 W, the bubbles' sizes can be adjusted to the desired values. Turning the laser power to 1.5 W, the stationary state can be realized when the bubble sizes are practically constant.

Visualization 2 shows that this two-fraction ensemble is equally stable in the perturbing liquid flow as was the spontaneously generated system of bubbles presented in Visualization 1. Remarkably, the bubbles of the large (diameter 40 mm) and small (15 mm) fractions are spatially distributed in agreement with the regularities described in Sec. 3.2.

5. Conclusion

We describe a method for controllable generation of vapor-gas microbubbles and their ensembles in water suspension with absorbing nanoparticles. The bubbles are formed under the action of the moderately focused near-infrared CW laser radiation which causes inhomogeneous heating of a thin suspension layer. After the suspension is properly superheated, the threshold conditions for the bubble generation are realized in the illuminated area, and they appear consecutively at random moments of time; when the heating is decreased below the threshold, formation of new bubbles is suppressed but the existing ones remain stable and can increase further, shrink or collapse depending on the incident laser power. This provides efficient means for regulation of the bubbles' number (from one to several tens) and sizes (including the possibility of creating several size fractions within a single ensemble).

The bubbles are kept together in the near-surface liquid layer within a limited area approximately corresponding to the bright spot of the focused laser beam. This is associated with the temperature excess necessary for the bubbles' existence and with the temperature dependence of the surface tension, which causes the bubbles to move towards the most heated region. However, the electric double layers formed at liquid–gas interfaces produce a sort of repulsive interaction that prevents the bubbles from coalescence and from adhesion to the water surface. As a result, quasi-ordered spatial distributions of bubbles are formed that are stable against mechanical perturbations caused, e.g., by the directional flow of the liquid. This feature opens interesting and valuable opportunities in the bubbles' manipulation techniques permitting easy and reliable ways for their transportation to a desired point inside an aqueous solution.

It should be noted that as in any case of inhomogeneous heating of a liquid-filled cell, the convection currents appear that also can contribute to the bubbles accumulation and ordering [34]. In our situation, the whole depth of the liquid is heated, and their influence is not so

strong as in the system of E. Flores-Flores et al. [34]. However, the heating is not perfectly symmetric, and horizontal convection is distinctly seen in Visualization 1 and Visualization 2. So far as we can judge from the actual experiments, the convection currents could not destroy the bubbles' adherence to the bright spot but effected certain redistribution of the bubbles of different fractions inside the spot (Fig. 7). It can be expected that the deliberate employment of the convection currents will supply additional efficient means for the more accurate localization and transportation of the bubbles but it is the task for future research.

Another interesting question concerns the bubbles' chemical composition that can differ from the air-vapor combination supposed in this paper, e.g., due to the laser-induced water splitting [35]. In our conditions of the CW irradiation and local heating below the critical temperature, chemical transformations, as a rule, do not occur; however this possibility can be especially important and, probably, helpful in practical situations where the bubbles perform selective localization and transfer of prescribed micro- or nanoobjects.

In general, the results of this paper can be useful for diverse applications dealing with the microbubbles and their systems, especially in association with the precise transportation and delivery of species in nano-engineering and in biomedical researches.

Acknowledgments